MINERALOGICAL MAGAZINE, SEPTEMBER 1986, VOL. 50, PP. 385–97

An electron optical study of muscovite breakdown in pelitic xenoliths during pyrometamorphism

A. J. BREARLEY

Department of Geology, The University, Manchester, M13 9PL

ABSTRACT. Transmission electron microscopy and analytical electron microscopy have been used to study the breakdown reaction of muscovite during pyrometamorphism. The transformation has been shown to be topotactic in nature, with the orientations of the product biotite and alkali feldspar being strongly controlled by the precursor phase. Microprobe investigations indicate that the reaction is probably isochemical with no detectable interaction with adjacent phases. Chemical analyses of the products carried out by AEM have enabled a possible balanced reaction to be calculated. It is proposed that the spatial distribution of the product minerals can be interpreted in terms of diffusion of species from one domain in the crystal to another over distances of 5 to 10 μm as a result of chemical potential gradients which develop during the reaction. The reaction probably occurred under conditions of declining temperature between 900 and 750 °C over a period of 4–5 days. This time period was insufficient to enable the reaction to reach completion as indicated by the presence of relics of muscovite coexisting with K-feldspar, corundum, biotite, hercynite, and mullite.

KEYWORDS: muscovite breakdown, electron microscopy, pelitic xenoliths, pyrometamorphism.

IN recent years transmission electron microscopy (TEM) has been increasingly used to study the mechanisms of mineral transformations on the microstructural level. Almost without exception these studies have been restricted to phenomena which occurred during the extended cooling histories of most igneous and metamorphic rocks, for example, exsolution, order–disorder transformations and reactions involving rehydration, e.g. Champness (1977), Putnis and McConnell (1980), Veblen and Buseck (1981), Veblen and Ferry (1984). These types of reaction are particularly suitable for study by TEM since the reactions take place within single crystals. It is, thus, comparatively simple to establish the relationships in terms of crystallography and chemistry of the phases and often to deduce a mechanism for the transformation. However, prograde reactions, which are of special relevance to metamorphic rocks, have been largely ignored, although some recent work has been done, e.g. Wirth (1985). The most obvious reason for this is the general absence of textural evidence of direct mineral reaction. Several authors, for example, Atherton (1965) and Carmichael (1969) have addressed themselves to this particular problem. The paucity of textural evidence of reactions in most regional metamorphic rocks, in particular, cannot be considered to be unusual in view of the extended periods of time which such rocks spend under conditions of elevated pressure and temperature. The kinetics of many metamorphic reactions are such that complete reaction will occur in the time scale of a regional metamorphic event. Hence direct, textural evidence of the progress of the reaction will be removed, particularly if water is readily available as a reactant and mass transport phase. It is probably only in the case of contact metamorphism that the periods of heating and cooling are sufficiently short to prevent complete reaction occurring. Thus in the contact aureoles of plutonic igneous rocks both reactants and products in a reaction may coexist. In such cases, e.g. Brearley (1984), the overall reaction can be deduced comparatively simply from light optical studies of textures. Nevertheless, the very earliest stages in the reaction may remain obscure. Reactions which have taken place under extreme conditions of contact metamorphism, e.g. pyrometamorphism, where the entire cycle of metamorphic events is highly compressed, are the most likely to have retained the earliest stages of the reaction and these may be revealed by TEM.

Sample locality and specimen description

The samples were collected from a Tertiary dolerite sill which outcrops on the south coast of the Ross of Mull between Scoor and Uisken (GR413 183), Isle of Mull, Argyll, Scotland. The sill is doleritic and belongs to the Loch Scridain suite of sills and dykes which occur in the southern part of Mull. It has a thickness of some 2 m and was intruded into a sequence of interbedded psammitic,

pelitic, and calcareous metasediments which may belong to the Glenfinnan division of the Moine series. Numerous xenoliths are found on the exposed upper surface of the sill and range in size from a few centimetres up to 1 m in diameter. All of the main Moine lithologies are found, although psammitic lithologies are predominant. Five samples were collected, three of which were subsequently selected for electron microprobe and electron microscope studies. The results from one pelitic xenolith collected some 20 cm from the edge of the sill are reported here.

Petrography

The optically observable assemblage in the xenolith is garnet + biotite + plagioclase + ilmenite. The presence of muscovite must largely be inferred by the presence of a dark fine-grained pseudomorph (see below). Quartz is absent in this sample, although it does occur in other xenoliths and in the Moinian metapelites adjacent to the sill.

Garnet occurs as large anhedral porphyroblasts up to 4 mm in diameter which have been partially pseudomorphed at the rims by an intergrowth of biotite, plagioclase, and ilmenite. This texture is commonly observed in garnets from the regional metamorphic gneisses of the Ross of Mull (Brearley, 1984) and is probably attributable to the retrograde breakdown of garnet during cooling. Electron microprobe analyses show that the garnets are predominantly an almandine–grossular solid solution with subordinate amounts of spessartine and pyrope. Compositions lie in the range $alm_{59}gr_{24}sp_{11}pyr_6$ at the cores to $alm_{67}gr_{16}sp_9pyr_8$ at the rims.

Plagioclase sometimes exhibits slight optical zoning with anorthite contents around An_{33} at the rims and An_{28} in the cores. Limited sericitization has been observed in some grains.

The original, dominant mineralogical constituents of the xenolith were muscovite and biotite which were present in modal quantities between 55 and 65% and preserve the original foliation of the pelitic gneiss. Optically, muscovite has been completely pseudomorphed by a fine-grained intergrowth of reaction products (fig. 1) which are found to exhibit weak pleochroic colours similar to those of biotite. No evidence of the precursor muscovite is usually observed, even when the rocks are examined at high magnification and its previous presence was initially inferred rather than positively identified. Pseudomorphing of the biotites in the same rock is not usually at such an advanced state as that of the muscovites. It exhibits considerable darkening in colour from deep reddish brown to almost black, particularly in the core regions. The rims of the biotites are usually lighter in colour, but are frequently mottled in appearance indicating a sub-microscopic intergrowth of phases. Ilmenite frequently occurs along the grain boundaries of the original muscovite and biotite crystals.

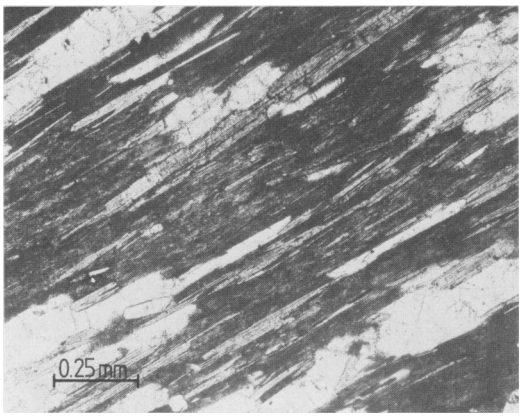

FIG. 1. Micrograph of dark pseudomorphs of muscovite coexisting with biotite and plagioclase (plane polarized light).

Attempts to identify the reaction products in the pseudomorphs of muscovite by electron probe microanalysis were unsuccessful due to the low spatial resolution of the electron beam.

Transmission electron microscopy

Experimental. Samples of muscovite pseudomorphs selected from doubly polished petrographic thin sections were thinned by ion-beam bombardment using the techniques outlined by Barber (1970) and Champness and Lorimer (1971). The specimens were subsequently examined in a Philips EM400T transmission electron microscope fitted with an EDAX energy dispersive X-ray spectrometer. A double-tilt goniometer stage fitted with a beryllium specimen insert (to minimize extraneous X-ray production during microanalysis) was used. All the observations were carried out at an accelerating voltage of 100 kV.

Observations. An extensive number of ion-thinned pseudomorphs of muscovite have been studied by TEM and a wide range of microstructures has been observed. These studies have enabled several different stages in the overall transformation to be identified, all of which can be observed within the area of a single thin foil.

The initial electron optical work established that the muscovites have only partially reacted, despite light optical observations to the contrary. Limited

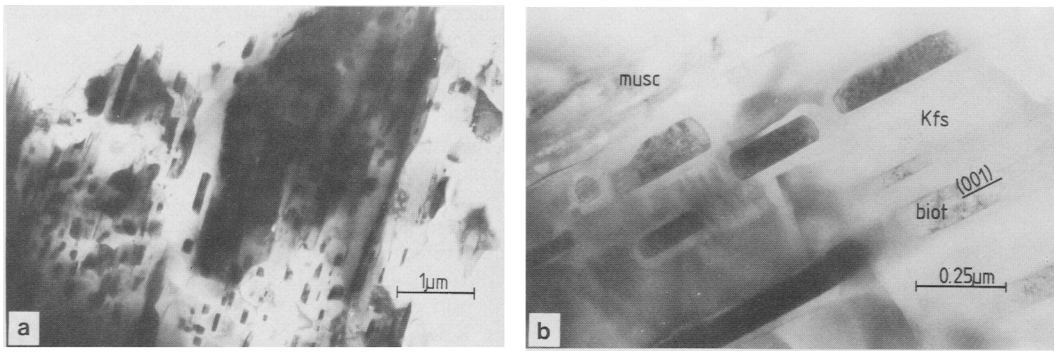

FIG. 2. (*a*) Transmission electron micrograph of an area of a muscovite pseudomorph consisting of numerous platelets of biotite within a matrix of K-feldspar and corundum. (*b*) Higher magnification micrograph of an area containing aligned (001) biotite platelets within K-feldspar. An area of beam-damaged precursor muscovite is present which has partially transformed to K-feldspar. The light-coloured haloes around the biotite particles are zones of electron-beam damaged feldspar.

areas of unreacted muscovite of limited spatial extent were found to occur adjacent to areas which have reacted extensively. The reaction products consist predominantly of particles of biotite which occur as aligned platelets parallel to $(001)_{biotite}$ (fig. 2*a* and *b*) within a matrix of monoclinic K-feldspar (sanidine). The size of these particles is highly variable, but they are typically 20–200 nm thick and invariably have curved ends (fig. 2*b*) and are 0.2–0.5 μm in diameter. Occasional errors in the (001) 10 Å lattice spacing have been observed in some particles; these are probably growth defects of the type observed by Bell and Wilson (1977) in metamorphic biotites. Imaged with the electron beam parallel to [001] the platelets have curved, irregular outlines and are usually 0.2–0.5 μm in diameter. The distribution of the particles within the pseudomorphs is highly variable with some areas of K-feldspar containing very low densities of platelets in comparison with the high densities shown in fig. 2*a* and *b*.

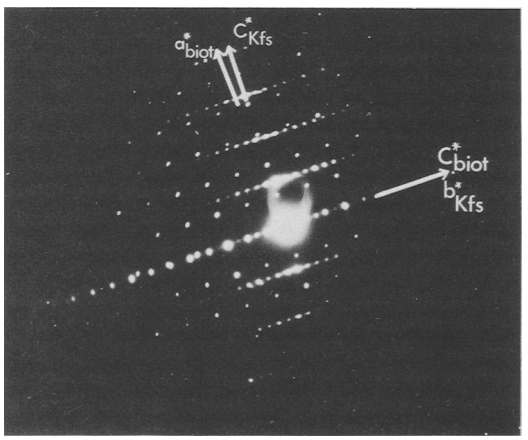

FIG. 3. Selected area electron diffraction pattern showing the crystallographic orientation relationship between biotite and K-feldspar.

The consistent parallel orientation of the biotite platelets indicates that the oriented sheet structure of the original muscovite has been retained by the biotite particles. It is these oriented biotite platelets which give rise to the weak pleochroic colours exhibited by the pseudomorphs in the light microscope.

Electron diffraction studies have shown that there is also a consistent orientation relationship between the K-feldspar and the biotite, i.e. $[010]_{biot} \parallel [100]_{kfs}$, $(001)_{biot} \parallel (010)_{kfs}$ (fig. 3). The occurrence of discrete (001) biotite platelets within K-feldspar is indicative of an advanced stage in the reaction, after extensive transformation of the muscovite has taken place.

In other regions of a single thin foil the very earliest stages in the reaction have also been observed. Areas of K-feldspar 0.03–0.04 μm apart develop within the muscovite parallel to the (001) plane (fig. 4). These areas are highly sensitive to electron beam irradiation and rapidly decompose to an amorphous reaction product. This instability may be due to a high local water content, which has a marked effect on the stability of many silicate minerals in the transmission electron microscope (Hobbs, 1983). Quantitative X-ray microanalysis of the beam-damaged areas yields Si/Al ratios which lie between 2.6 and 2.9 and are broadly consistent with K-feldspar. However, the K_2O contents are

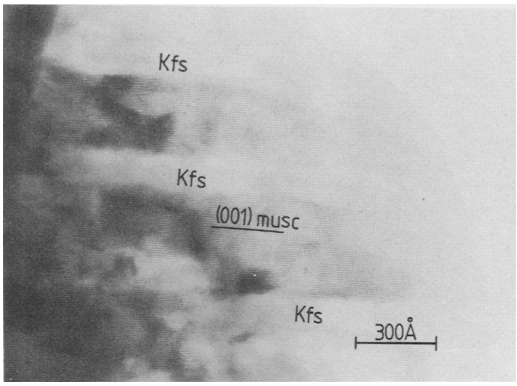

FIG. 4. One-dimensional (001) lattice image of an area of muscovite in the earliest stages of the reaction. Alkali feldspar is developing in areas about 0.04 μm apart parallel to the (001) basal plane of the muscovite. The feldspar in these areas is highly unstable in the electron beam and has partially decomposed to an amorphous phase, possibly as a result of a high local water content.

always low (< 3 wt. %). This spread in Si/Al ratios is probably attributable to the very low count rates (and hence poor statistics) obtainable from these areas due to their very limited spatial extent. This necessitates the use of a highly focused electron probe for the analysis which creates substantial problems with elemental mass volatilization of K_2O. The low K_2O values can be accounted for by this effect which is discussed in more detail later. Some variation in the Si/Al ratios of the K-feldspar may also result from X-ray contributions from the adjacent muscovite which has Si/Al values of between 1.35 and 1.6.

Volumetrically, K-feldspar and the platelets of biotite are the most important product phases in the cores of the pseudomorphs. However, hercynitic spinel (pleonaste), a product phase of some significance, has also been identified by TEM.

The earliest stage in the formation of hercynite is the development of regions of an amorphous phase, typically 0.4 μm in diameter and containing Mg, Fe, and Al, which occur, without exception, in the K-feldspar (fig. 5*a*). These amorphous areas occur in groups and probably formed contemporaneously with the K-feldspar. They are, effectively, areas of excess material, released from the breakdown of the precursor muscovite and may originally have been areas of melt. Hercynite nucleates within these areas as numerous (20–30), unoriented, euhedral crystals about 0.05 μm or less across (fig. 5*b*).

High-resolution direct-lattice imaging of the particles has revealed further information about the possible mechanisms of nucleation and growth. Many of the hercynite crystals are found to be twinned on {111} according to the spinel twin law. The lattice image (fig. 6*a*) of the twin plane shows that it consists of a disordered sequence of up to five microtwins one structural unit thick, rather than a single, discrete twin plane. It is probable that this disordered sequence represents the original nucleus of the crystal and constitutes a set of nucleation twins of the type discussed by Whittaker (1981). The nucleus may have a somewhat different structure from the ordered crystal which grows either

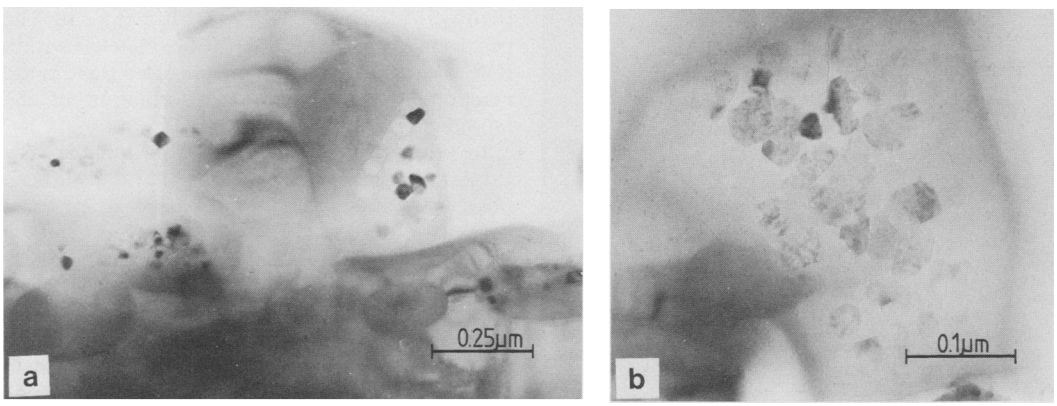

FIG. 5. (*a*) Micrograph of an area of alkali feldspar containing several groups of hercynite crystals in their earliest stages of growth. (*b*) Higher magnification micrograph of a single group of hercynite particles within an amorphous matrix. The particles are usually euhedral and have random orientations (evident from the wide variation in diffraction contrast between the individual crystals).

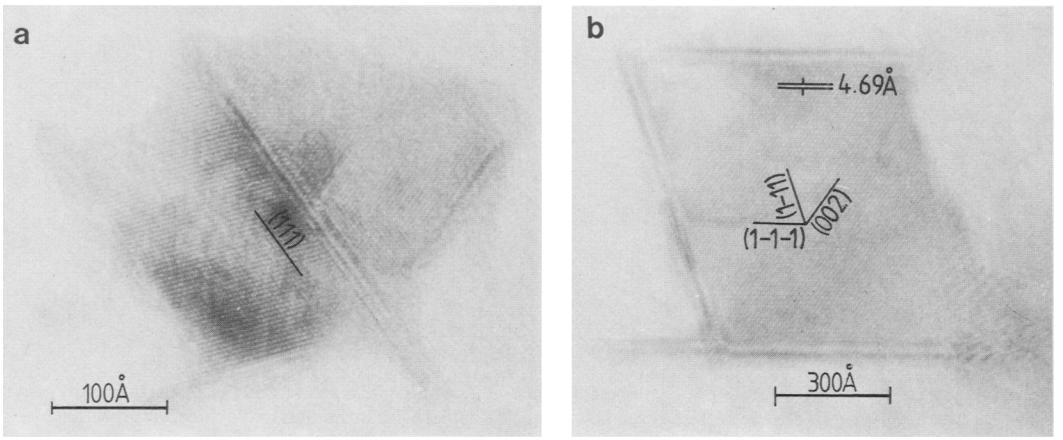

FIG. 6. (*a*) Hercynite particle exhibiting a twin boundary which consists of 5 microtwins in the centre of the crystal. The composition plane is (111) (spinel twin law). Note also the growth fins parallel to (111). (*b*) High-resolution, 2-dimensional direct lattice image of euhedral hercynite particles imaged with the electron beam approximately parallel to the [110] zone axis. Lattice periodicities corresponding to the 4.65 Å (111) and 4.02 Å (002) planes are imaged. Growth 'fins' radiating from the corners of the crystals are present parallel to the (111) plane.

side of the twin boundary and probably has higher 2-dimensional symmetry.

Many of the hercynites have fins growing from their corners parallel to the {111} faces (fig. 6*b*). Dendrites of this type are indicative of rapid growth from a supersaturated solution (McClachlan, 1978) such as a melt or amorphous solid. The effect of supersaturation is to lower the activation energy for nucleation and is also consistent with the occurrence of a large number of small crystals, i.e. simultaneous nucleation at a large number of sites.

After the earliest stages of development, hercynite growth probably occurs by a classical coarsening mechanism with the largest crystals growing at the expense of smaller ones. This effectively lowers the total surface free energy of the system. With progressive coarsening hercynite crystals up to 1.5 μm in diameter develop (fig. 7). They occur in groups of four to five crystals with well-formed faces indicative of a close approach to textural equilibrium. This is evidently an advanced stage in the overall reaction and was only very infrequently observed in the thin foils.

Corundum is one of the other main reaction products in the muscovite pseudomorphs and occurs in two distinct habits. It is found sporadically as subhedral, elongate crystals (0.1–0.5 μm in diameter) within the intergrowths of K-feldspar and biotite platelets and also occurs as acicular crystals within areas of K-feldspar where biotite is not abundant. There is no crystallographic relationship between corundum and the biotite or K-feldspar.

The other aluminosilicate phase which occurs in the muscovite pseudomorphs is mullite. It occurs as numerous, slightly curved, acicular needles, similar in morphology to the corundum needles, and lies parallel or subparallel to the intergrowth of K-feldspar and biotite (fig. 8*a*). Although the mullite needles have a morphological preferred orientation, electron diffraction studies show that the majority of the crystals have no lattice orientation relationship with the K-feldspar. Some crystals, however, have the crystallographic relationship with the K-feldspar $[213]_{mull} \parallel [\bar{2}01]_{Kfs}$, $(2\bar{1}\bar{1})_{mull} \parallel (010)_{Kfs}$.

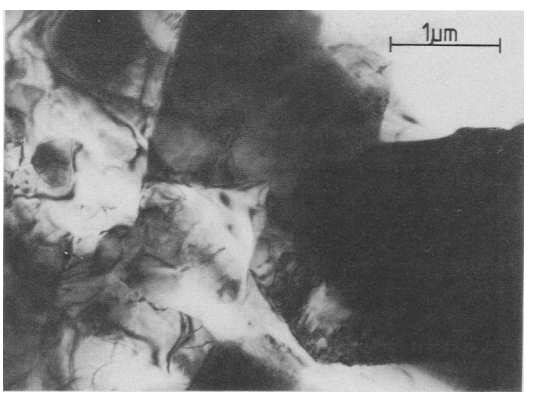

FIG. 7. Group of well-crystallized, euhedral hercynite particles.

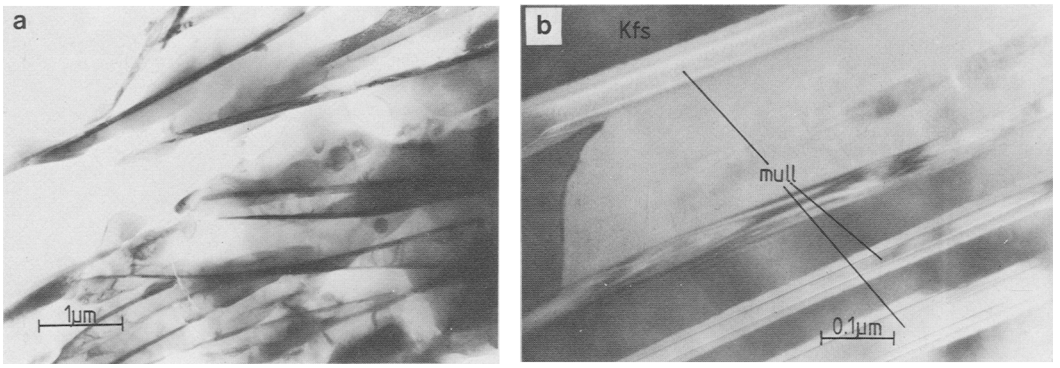

FIG. 8. (*a*) Area of K-feldspar containing acicular crystals of mullite. Hercynite is absent and biotite particles only occur sporadically. (*b*) Oriented acicular mullite crystals within K-feldspar. Discontinuous microtwins occur parallel to *c* (mullite).

Discontinuous microtwins (fig. 8*b*) have also been observed in some mullite crystals. Electron diffraction has confirmed that these are (001) microtwins similar to those observed by Nakajima and Ribbe (1981) in synthetic Al-rich mullites.

Mineral chemistry

Experimental. Chemical data for the phases involved in the reactions has been obtained by analytical electron microscopy (AEM) using the thin film approximation of Cliff and Lorimer (1975) to quantify the results. This method calculates elemental concentrations from the ratio of X-ray intensities rather than by the comparison of absolute concentrations, the technique used in electron probe microanalysis. Corrections were made for secondary fluorescence and absorption although both effects are minimal. All the analyses must therefore be normalized to 100%, preventing any estimation of the water content of hydrous phases.

K-feldspar. The analysis of alkali feldspars in the TEM is subject to the considerable problem of alkali volatilization induced by the electron beam. This loss is a well-documented problem in electron microprobe analysis (Smith and Ribbe, 1966) and is even more acute in thin-film microanalysis, where finely focused electron probes accentuate the rate of volatile loss.

Feldspar analyses carried out at 100 kV using a beam diameter of 0.04 μm were found to exhibit K and Na losses of between 20 and 80% of the total. Even using a broadened probe of about 0.2 μm diameter, more than 2 wt. % K_2O was lost during an analysis over 60 sec analytical live-time. This problem was tackled in a similar way to that described by McGill and Hubbard (1981) for the analysis of orthoclase and albite.

A series of analyses at 60 sec live-time intervals up to a total of 360 sec was carried out on a single spot using a 0.1 μm probe diameter. Between each analysis the beam was spread to avoid K-loss during the processing of the data. The results are shown in fig. 9*a*, where the Al/Si and K/Si ratios are plotted against analytical live-time. The Al/Si ratio during this period remains unchanged, but K/Si decreases by almost 50%. In fig. 9*b* these data are shown in terms of the K_2O loss for the same irradiation time. Even using operating conditions least likely to induce volatilization whilst retaining reasonable spatial resolution, about 2 wt. % K_2O is lost during the first 60 sec. After about 300 sec irradiation time the rate of K loss levels out and perhaps indicates that, for a given set of operating conditions, there is a limit to the amount of volatilization that can occur. An extrapolation back to zero live-time gives an approximate value of the initial K_2O value of 13 wt. % for this example and a range of values from the other analyses of 12.5 to 14.5 wt. % K_2O. A similar plot of Na_2O results in intercepts of between 1.5 and 2.5 wt. % Na_2O. The recalculated formulae based on these data yield reasonable stoichiometry, despite the assumptions made. The resultant compositions of the K-feldspars lie between $Or_{85}Ab_{15}$ and $Or_{75}Ab_{25}$.

Biotite. AEM analyses of the biotite platelets and electron microprobe analyses of regional metamorphic biotites with total iron calculated as FeO are reported in Table I*a* and *b*. All the analyses have been recalculated on the basis of 22 oxygen atoms. The biotite particles are compositionally diverse, as illustrated in two plots, fig. 10*a* and *b*. Fig. 10*a* is simply a plot of Si *vs.* Al (cation proportions) for

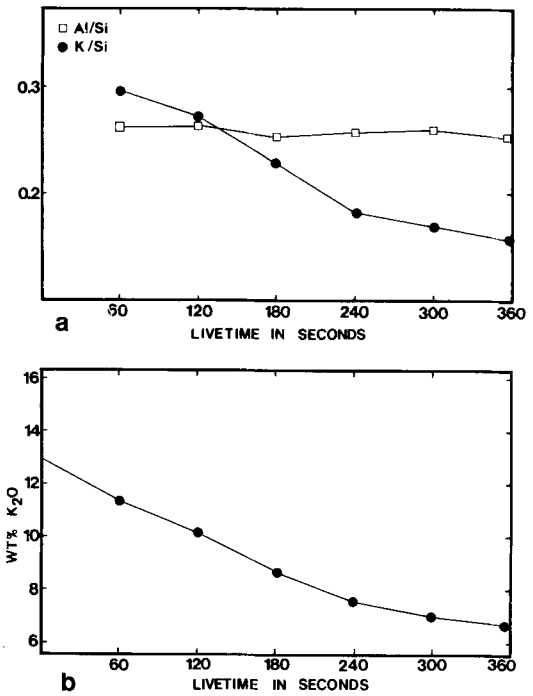

FIG. 9. (*a*) Plot of Al/Si and K/Si ratios (element %) as a function of analytical live-time (sec) for potassium feldspar during microanalysis in the TEM. (*b*) Plot of K_2O (wt. %) from potassium feldspar as a function of analytical live-time (sec) during microanalysis in the TEM.

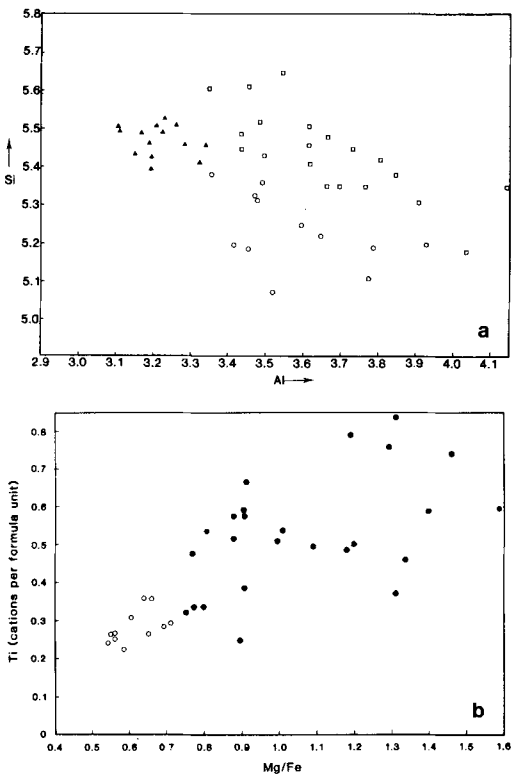

FIG. 10. (*a*) Plot of Si *vs.* Al (cations based on 22 oxygen atoms) for biotite particles in the muscovite pseudomorphs. Open squares = biotites coexisting with K-feldspar, corundum, and hercynite; open circles = biotites coexisting with mullite; triangles = microprobe analyses of regional metamorphic biotites. (*b*) Plot of Ti content (cations) *vs.* Mg/Fe ratio for biotite platelets (closed circles) from the muscovite pseudomorphs. Open circles are microprobe analyses of regional metamorphic biotite.

all the analysed biotites. Some electron microprobe analyses of regional biotites are also shown.

The biotite particles show a wide range of Si/Al ratios, but are almost invariably Si-deficient and Al-enriched relative to the microprobe analyses of regional biotite. Furthermore the platelets which coexist with corundum are usually significantly more aluminous than those which coexist with mullite for an equivalent Si content.

Accurate determination of the potassium contents of the biotites is difficult due to mass volatilization problems similar to those encountered with the alkali feldspar discussed above. However, this problem does not seem to be as acute for biotite except for particles at the lower end of the size range when a highly focused electron probe must be utilized for the analysis. In this extreme situation the alkali site occupancy calculated on the basis of 22 oxygen atoms may be as low as 1.3–1.4 indicating a substantial potassium loss. Analyses of larger particles (150–200 nm in thickness) usually yield site occupancies of between 1.6 and 1.8, data which are comparable with results from the electron microprobe for the regional metamorphic biotites (Table I*b*).

A particularly notable variation in biotite chemistry is shown by their Mg/Fe ratios and Ti contents as shown in fig. 10*b*. Regional biotites have low Mg/Fe ratios and low Ti contents in comparison with biotite platelets in the muscovite pseudomorphs, which exhibit a wide range of values with Mg/Fe up to 1.6 and Ti in excess of 0.8 cations (8–9 wt. % TiO_2). Within the analyses of biotite platelets there is an indication that the Mg/Fe ratios increase with increasing Ti content, although there is a marked spread in the data. However, this is consistent with the observations of Guidotti *et al.* (1975) who showed, on crystal chemical grounds, that the Ti contents of biotite

Table Ia. Representative AEM analyses of biotite platelets

SiO_2	39.39	38.81	38.94	36.74	37.02
TiO_2	3.39	4.88	4.08	5.57	7.26
Al_2O_3	18.24	21.79	22.65	23.57	22.86
FeO	20.63	16.33	15.04	16.33	13.21
MnO	0.18	-	-	0.09	-
MgO	8.47	9.12	9.91	8.26	9.43
CaO	-	-	-	-	-
Na_2O	-	-	-	-	-
K_2O	9.70	9.07	9.38	9.44	10.22
Total	100.00	100.00	100.00	100.00	100.00
FORMULA BASED ON 22 [O] ATOMS					
Si	5.688	5.455	5.443	5.194	5.187
Ti	0.368	0.515	0.429	0.582	0.765
Al	3.105	3.611	3.732	3.929	3.776
Fe	2.491	1.919	1.762	1.931	1.548
Mn	0.022	-	-	-	-
Mg	1.822	1.906	2.064	1.740	1.969
Ca	-	-	-	-	-
Na	-	-	-	-	-
K	1.785	1.626	1.664	1.699	1.825

Table Ib. Microprobe analyses of regional biotites

SiO_2	35.46	35.07	35.61	35.18	35.63
TiO_2	3.38	2.89	1.98	3.04	2.68
Al_2O_3	17.69	17.52	17.49	17.05	17.29
FeO	21.04	22.85	22.78	22.96	22.32
MnO	-	0.20	-	-	-
MgO	8.05	7.22	8.26	7.48	7.66
CaO	-	-	-	-	-
Na_2O	0.63	-	-	0.44	-
K_2O	9.04	94.41	94.68	95.59	94.21
Total	95.31	94.41	94.68	95.59	94.21
FORMULA BASED ON 22 [O] ATOMS					
Si	5.445	5.471	5.519	5.460	5.542
Ti	0.391	0.339	0.232	0.355	0.313
Al	3.202	3.222	3.196	3.118	3.169
Fe	2.702	2.981	2.953	2.979	2.903
Mn	-	0.027	-	-	-
Mg	1.843	1.678	1.908	1.730	1.776
Ca	-	-	-	-	-
Na	0.189	-	-	0.133	-
K	1.771	1.721	1.691	1.778	1.714

increase as a function of Mg/Fe ratio. The very high Ti contents may also reflect the expansion of the solubility of Ti in biotite as a function of temperature, as observed by Roberts (1975) experimentally and by other workers on natural biotites, e.g. Kwak (1968).

Hercynites. Representative analytical data from AEM for hercynites are presented in Table II with formulae calculated on the basis of 32 oxygen atoms. Some of the formulae calculated on the basis of total Fe as FeO were found to exhibit very poor stoichiometry with total cations over 24. This has been attributed to the occurrence of Fe^{3+} in the structure, i.e. the presence of magnetite in solid-solution in the spinel. These formulae were recalculated reiteratively assuming a cation sum of 24 and site occupancies of 8 and 16 for the *A* (fourfold co-ordination) and *B* (sixfold) sites respectively. Satisfactory formulae were usually obtained by this data reduction procedure and indicate that between 1 and 5% of total iron may be present as Fe^{3+}.

Table II. Representative AEM analyses of hercynites

SiO_2	1.77	-	-	-
TiO_2	0.55	0.13	1.56	0.18
Al_2O_3	64.02	61.67	60.85	59.39
Fe_2O_3	-	0.78	-	1.55
FeO	24.54	28.37	31.10	33.53
MnO	0.25	-	0.30	0.27
MgO	8.87	9.05	6.19	5.08
Total	100.00	100.00	100.00	100.00
FORMULA BASED ON 32 [O] ATOMS				
Si	0.373	-	-	-
Ti	0.088	0.021	0.255	0.030
Al	15.940	15.818	15.784	15.730
Fe^{3+}	-	0.130	-	0.194
Fe^{2+}	4.335	5.082	5.783	6.300
Mn	0.045	0.024	0.058	0.049
Mg	2.786	2.925	2.031	1.701

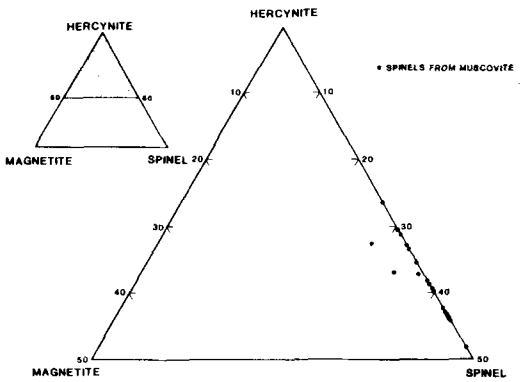

FIG. 11. Spinel compositions from muscovite pseudomorphs in part of the ternary system hercynite–magnetite–spinel.

These data are presented in fig. 11 in part of the ternary system hercynite ($FeAl_2O_4$)–magnetite ($Fe^{2+}Fe_2^{3+}O_4$)–spinel($MgAl_2O_4$). The chemical data are widely distributed, but show that the compositions are dominantly hercynitic in composition with usually greater than 55 mol. % hercynite. The majority of the analyses are compositionally restricted to the hercynite–spinel join and contain little or no magnetite. There is no evidence of any compositional distinction between the small and large hercynite crystals.

Mullites. AEM analyses of mullite from the muscovite pseudomorphs show that it has a variable chemistry. Representative analyses which cover this range of compositions are presented in Table III with the formulae calculated on the basis of 13 oxygen atoms. Stoichiometric mullite is generally accepted to have the composition $3Al_2O_3 \cdot 2SiO_2$, but has been shown by Cameron (1977) to have a range of solid-solution between sillimanite and peraluminous mullites which tend towards ι-Al_2O_3 in composition. The extent of this compositional range known to date can be

Table III. Representative AEM analyses of mullite

SiO_2	27.07	26.59	25.02	25.27	22.53
TiO_2	1.45	1.78	1.25	-	1.48
Al_2O_3	68.39	70.33	72.44	73.84	74.86
Fe_2O_3	3.14	1.28	1.28	0.87	1.22
Total	100.00	100.00	100.00	100.00	100.00
	FORMULA BASED ON 13 [O] ATOMS				
Si	1.942	1.902	1.792	1.788	1.619
Ti	0.078	0.086	0.067	-	0.080
Al	5.800	5.931	6.117	6.234	6.334
Fe^{3+}	0.170	0.069	0.069	0.047	0.066
Sum	7.992	7.988	8.046	8.070	8.099

described in terms of the formula $Al_{4+2x}Si_{2-2x}O_{10-2x}$ where x can lie between 0.17 and 0.59. The extent of solid solution observed in natural mullites is, however, restricted to a very limited range where x lies between 0.17 and 0.20 corresponding to 57.5 and 60 mol. % Al_2O_3. The full range of mullite compositions is only obtainable under high-temperature experimental conditions, usually quenched from melts (Cameron, 1977). However, the present study suggests that, under special disequilibrium conditions, natural mullites with $x > 0.20$ can form.

The compositional variation of mullites from the muscovite pseudomorphs is illustrated in fig. 12, which shows a plot of Si *vs.* Al based on 13 oxygen atoms. The mullites clearly exhibit a wide range of compositions from 5.6 to 6.6 Al cations per formula unit. There is some scatter in the data, but it is largely removed by including Ti and Fe^{3+} with Al. In terms of mullite compositions normalized to $Si + Al = 6$, this range corresponds to an Al content of between 4.35 and 4.95 cations, i.e. $x = 0.17$ to 0.475. Very few of the analyses lie close to stoichiometric mullite. The majority are exceptionally peraluminous with between 31.5 and 39 mol. % SiO_2. This is clearly a very marked extension of the solid solution range observed to date in natural mullites.

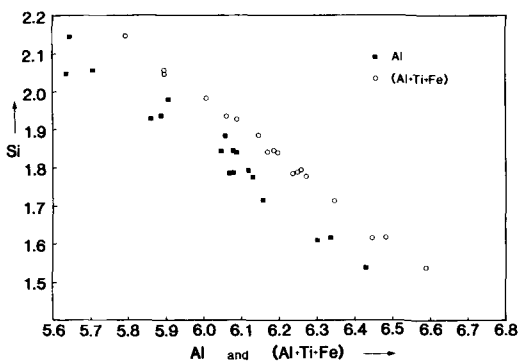

FIG. 12. Si *vs.* Al and Si *vs.* $(Al + Ti + Fe^{3+})$ for mullites analysed in the TEM.

Reaction mechanism

The breakdown of muscovite can be considered as taking place essentially by the partial pseudomorphing of the precursor crystal, a reaction which may or may not involve some interaction with adjacent phases. In order to assess the extent of cation exchange between coexisting phases, electron microprobe traverses were carried out across interfaces between the muscovite pseudomorphs and plagioclase and biotite. No zoning could be detected using a 2 μm probe diameter. This would imply no net exchange of species between any of the phases. The breakdown of muscovite appears, therefore, to have been isochemical in nature and the bulk compositions of the pseudomorphs can reasonably be regarded to be that of the precursor muscovite.

Table IV. Microprobe analyses of phengite.

SiO_2	51.33	52.17	49.75	48.77
TiO_2	1.44	1.16	1.52	1.13
Al_2O_3	27.56	29.19	30.10	28.96
FeO	2.56	2.22	2.51	2.36
MnO	-	0.11	-	0.15
MgO	1.49	1.34	1.25	1.13
CaO	-	0.09	0.17	0.15
Na_2O	1.05	1.47	0.88	1.19
K_2O	9.75	10.08	10.37	10.26
Total	95.17	97.85	96.66	94.24
	FORMULA BASED ON 22 [O] ATOMS			
Si	6.838	6.766	6.505	6.633
Ti	0.145	0.113	0.150	0.115
Al	4.330	4.460	4.682	4.683
Fe	0.280	0.240	0.280	0.260
Mn	-	0.012	-	0.017
Mg	0.296	0.260	0.246	0.228
Ca	-	0.013	-	0.021
Na	0.271	0.372	0.225	0.314
K	1.657	1.668	1.693	1.773

The compositions of a number of pseudomorphs has been determined by microprobe analyses using a 10 μm probe diameter to minimize elemental mass volatilization of alkalis. Typical microprobe analyses are reported in Table IV and show that the precursor muscovites were highly siliceous, unusually so for muscovites found in the Moinian rocks of the Ross of Mull. There is a considerable variation in the chemistry of these muscovites, which are essentially phengitic in character. Mg/Fe ratios vary between 0.75 and 1.1 and Si ranges between 6.4 and 6.8 cations per formula unit. The phengites are also fairly paragonitic [Na/(Na + K) = 0.14–0.18] and the alkali site sometimes contains in excess of 2 cations per formula unit. This is slightly problematical and may be

due to difficulties of sodium analysis on the microprobe.

Because of the considerable compositional variation evident in the muscovite pseudomorphs, the composition of the product phases will also vary. Consequently a balanced reaction has been calculated based on a muscovite pseudomorph for which bulk compositional data from the electron microprobe and analytical data for the product phases from the TEM are available. All the other compositional variations exhibited by the product biotites, hercynites and mullites are probably attributable to variations in the precursor phengite compositions.

Four lines of textural and chemical evidence have been used to develop a possible reaction for the breakdown of phengite. These are:

(1) Where particles of biotite are most abundant, K-feldspar and corundum are invariably the coexisting phases. Hercynite is present as a minor phase but no mullite is found.
(2) Where mullite occurs biotite is volumetrically only a minor phase.
(3) Corundum and mullite are rarely found coexisting.
(4) The analytical data for the biotite particles coexisting with corundum, K-feldspar, and hercynite have Mg/Fe ratios which are close to those of the precursor phengite as determined by electron microprobe. In contrast the biotites which coexist with mullite are significantly more Mg-rich than the phengite.

These data imply that there are two separate reactions which occur in adjacent coupled diffusion domains within the crystal. The products of the reaction and their compositions are different in each of these domains and the overall reaction may involve mass transfer between the two distinct regions.

This mechanism is similar in some respects to the model of Carmichael (1969) for reactions in regional metamorphic rocks except that the diffusion domains are markedly smaller in this instance. Volume diffusion is the dominant mass transfer mechanism rather than diffusion of ionic species through the grain boundary network.

The first reaction based on the observed association of phases has been deduced to be:

$$\text{phengite} = \text{K-feldspar} + \text{biotite} + \text{corundum} + \text{hercynite}. \quad (1)$$

The reaction based on one mole of phengite is shown in fig. 13. The amount of biotite produced in the reaction is controlled by the amount of Ti, Mg, and Fe in the precursor phengite and is therefore calculated first in the reaction scheme followed by calculation of the amount of K-feldspar. The Mg/Fe ratio of the product biotite is the same as that for the precursor phengite and all the Na and remaining K are allocated to the alkali feldspar. This leaves no residual Mg and Fe to form hercynite, but results in an excess of Si and Al. The main problem is the allocation of Si left over from

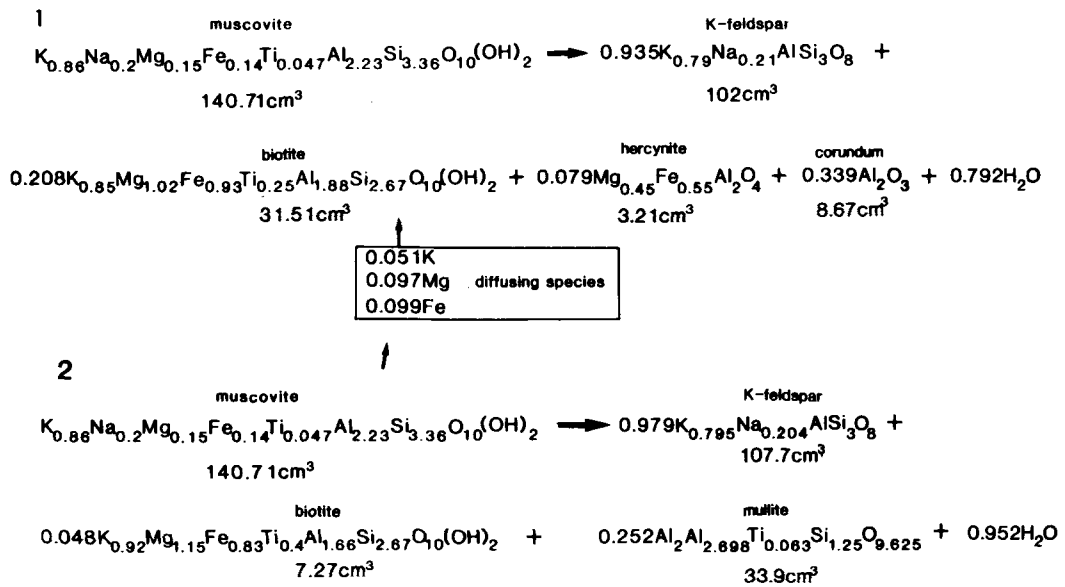

Fig. 13. Possible balanced reaction scheme for the breakdown of muscovite, in two adjacent diffusion domains within the single crystal.

the reaction. If the residual cations are assumed to form mullite it would have an exceptionally peraluminous composition with Si/Al ratios of between 0.14 and 0.18. This range of ratios corresponds to mullites with 22–27 mol. % SiO_2. No mullites with this composition have been found in the pseudomorphs: all the analysed mullites have compositions lying between 31 and 38 mol. % SiO_2. This is clearly a marked discrepancy.

The textural evidence indicated in points 1, 2, and 3 above has been used to deduce a possible reaction which enables an allocation of the residual cations to be made.

Once K-feldspar and biotite have nucleated in the reacting muscovite, growth will proceed rapidly at the prevailing high temperature. This will have the effect of establishing chemical potential gradients in the matrix around the growing biotite particles with Ti, Mg, Fe, and K diffusing to the growth interface. Because volume diffusion of Al is generally considered to be comparatively sluggish (Anderson and Buckley, 1973) no extensive movement of Al is invoked here, although it is possible that some Si diffusion may have occurred.

At this stage the growth of biotite will probably be diffusion controlled. It is difficult in practice to establish the distances over which diffusion is likely to have taken place but it may be of the order of 10 to 15 μm. The residual Si is likely to be involved in this biotite-forming reaction and leaves the remaining Al to produce corundum. The high local chemical potential of Al probably results in the formation of hercynite during the period of biotite growth, but only in limited amounts. An examination of the Mg/Fe partitioning between hercynite and biotite indicates that K_D is approximately constant. This is shown in fig. 14 and suggests that equilibrium between the two phases was almost achieved. It is also worth noting that no biotites with Mg/Fe ratios greater than the maximum Mg/Fe ratio of the phengites has been found coexisting with hercynite. Only the biotite particles coexisting with mullite have Mg/Fe ratios which are markedly higher.

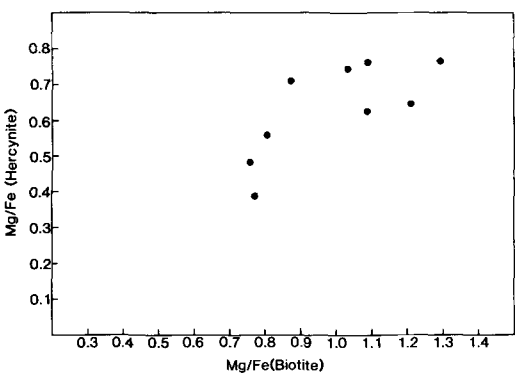

FIG. 14. Plot of Mg/Fe ratios for coexisting hercynites and biotites from muscovite pseudomorphs.

Constructing a balanced reaction involving the formation of hercynite is difficult because the volume of hercynite produced is not known accurately and is a function of the time over which diffusion has operated. Because of this uncertainty, the volume of hercynite has been arbitrarily chosen as 2.5% of the total volume of the reaction products.

The development of mullite can now be considered in the second reaction domain which has lost Mg, Fe, Ti, and K. This reaction is considered as the second part of the reaction (1) which can be schematically regarded as:

$$\text{phengite} = \text{K-feldspar} + \text{biotite} + \text{mullite}. \quad (2)$$

The starting composition of the muscovite is assumed to be the same as reaction (1), i.e. the muscovite crystals are chemically homogeneous and the number of cations used in reaction (1) are subtracted. From the residual cations a biotite composition of that coexisting with mullite is initially calculated followed by K-feldspar. The remaining Si and Al produce mullite which has a composition containing 38.5 mol. % SiO_2, i.e. a composition which is consistent with that determined by AEM. The complete balanced reaction scheme involving reaction (1) and (2) is shown in fig. 13.

It is also useful here to consider the volume changes for the solid phases in the reaction. Using the 1 bar 298 K molar volume data either from Helgeson *et al.* (1978) or Robie *et al.* (1978) an approximate volume change for the reaction can be calculated. This gives a net volume increase of 4.6 cm^3 for reaction (1) and an increase of 8.6 cm^3 for reaction (2) from 1 mole of muscovite. This is a small increase and could be rather lower if the molar volume of the phengite were known accurately.

Discussion

The chemical and electron optical data show that equilibrium was not established on the scale of a single muscovite crystal, although locally, perhaps on a scale of 5–10 μm, equilibrium may have been approached. The reaction has not gone to completion as is indicated by the occurrence of relics of muscovite still persisting in some areas.

The actual time available for the reaction can be estimated from the heat flow data of Jaeger (1957). If the magma is assumed to have been intruded at

1000 °C and to have crystallized at 800 °C, a probable maximum temperature reached by the xenolith is about 900 °C. Within about 4 days the temperature is likely to have dropped to 770 °C and subsequently the drop in T took place rather more slowly.

According to the experimental data of Chatterjee and Johannes (1974) the muscovite breakdown reaction occurs at around 570 °C at 1 kbar. In practice the breakdown curve of phengite is likely to be at a rather lower temperature, but the data imply an overstepping temperature ΔT of the order of 350–400 °C, a very marked departure from equilibrium. The rate at which this maximum overstepping temperature was reached is likely to have been rapid and to have occurred shortly after the injection of the sill. Nucleation may have commenced during this increase in temperature at nucleation sites which are energetically the most favourable, i.e. in this case grain boundaries, dislocations and other crystallographic defects. These sites make a negative contribution to the free energy needed to form a nucleus of critical size, i.e. the nucleation occurs by a heterogeneous mechanism. The actual number of nucleii which form is dependent on two factors, the nucleation rate and the time for which nucleation has operated. Although the nucleation rate changes very rapidly as a function of temperature if the rate of increase in temperature (dT/dt) is sufficiently fast, the number of nucleii which form during the heating event may be of limited number. Classical nucleation theory (Christian, 1975) predicts that the nucleation rate will eventually attain a quasi-steady state, but until that state is reached the nucleation rate is a function of time. Data from metallurgical systems suggest that when reactions occur during supercooling a period of incubation elapses before nucleation commences. It is not clear to what extent this occurs during superheating reactions, but it is probably not significant.

In the case of pyrometamorphism it is highly unlikely that the steady state condition will ever be reached. The rate of nucleation will lag behind the change in temperature during the up-temperature path until the maximum temperature is reached. The peak metamorphic temperatures are unlikely to be maintained for any substantial time before cooling commences.

The rate of cooling is substantially less than the rate of temperature increase and it is probable that the majority of nucleii will be formed during this cooling history under almost isothermal conditions. The number of nucleii produced will decrease rapidly as the temperature falls and at the same time the overall transformation rate will become increasingly sluggish. The period of time over which nucleation occurs is probably a substantial fraction of the total available time for the transformation and this has the effect of preserving various stages of the reaction within the same

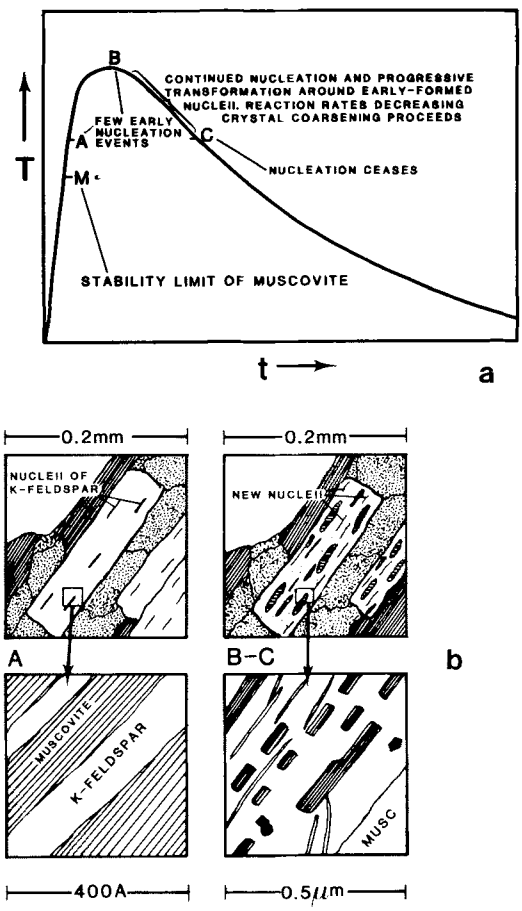

FIG. 15. (*a*) Hypothetical temperature-time path for the reacting muscovite. During the initial heating the muscovite reaction curve is overstepped until nucleation begins at point A. Few nucleii are formed between A and B, the maximum temperature attained. More nucleii form during the longer cooling history, whilst areas which started to transform between A and B continue to react and the phases coarsen. Nucleation probably ceases at around C or possibly before. (*b*) Schematic representation of the evolution of the reaction microstructure as a function of time for the stages A to B and B to C on the time-temperature curve in fig. 15*a*. Stipled phase = plagioclase, parallel lines = biotite. Muscovite is white with elongate nucleii of K-feldspar developing along (001) muscovite between A and B. This continues between B and C, with the corresponding microstructure showing development of biotite particles (parallel lines), hercynite (dark) and needles of mullite within K-feldspar (white).

crystal. Areas of phengite which began to transform during the increase in T have had a longer period of time to transform than areas where nucleation commenced during cooling.

It is a simplification to consider the activation energy for nucleation as being identical for all the phases involved in a discontinuous reaction. In practice the free energy involved in forming a nucleus will be different for each phase, and so the nucleation rate for each phase will also be different. In the case of mullite and corundum nucleation appears to have been controlled by the presence of interfaces between K-feldspar and biotite. These latter two phases have a strong crystallographic orientation relationship, which has been controlled by the crystallography of the precursor muscovite. It is possible that nucleation of mullite or corundum could not take place until an interface was present to act as a very low energy nucleation site.

Once nucleation has taken place growth will almost certainly be the rate-determining step, with the overall reaction rate being controlled by the diffusion of the slowest species.

To summarize the overall reaction history a hypothetical temperature-time path for the reacting muscovite and schematic representations of the evolution of the microstructure at various stages during the reaction are shown in fig. 15*a* and *b*.

Acknowledgements. The author would like to thank Graham Cliff, Ian Brough, and Pete Kenway of the Joint Umist/Manchester University Metallurgy Department for technical assistance with the TEM work, and Dr P. E. Champness for her valuable comments on the manuscript. This work was carried out while the author was in receipt of an NERC Research Studentship which is gratefully acknowledged.

REFERENCES

Anderson, D. E., and Buckley, G. R. (1973) *Contrib. Mineral. Petrol.* **40,** 87–104.

Atherton, M. P. (1965) In *Controls of metamorphism* (W. S. Pitcher and G. W. Flinn, eds.). Oliver and Boyd, Edinburgh.

Barber, D. J. (1970) *J. Mater. Sci.* **5,** 1–8.

Bell, I. A., and Wilson, C. J. L. (1977) *Phys. Chem. Mineral.* **2,** 153–69.

Brearley, A. J. (1984) Unpubl. Ph.D. thesis, Univ. of Manchester.

Cameron, W. E. (1977) *Am. Mineral.* **62,** 747–55.

Carmichael, D. M. (1969) *Contrib. Mineral. Petrol.* **20,** 244–67.

Champness, P. E. (1977) *Ann. Rev. Earth Planet. Sci.* **5,** 203–26.

—— and Lorimer, G. W. (1971) *Contrib. Mineral. Petrol.* **33,** 171–83.

Chatterjee, N. D., and Johannes, W. (1974) Ibid. **48,** 89–114.

Christian, J. W. (1975) *Transformations in metals and alloys. I. Equilibrium and general kinetic theory.* Pergamon Press, Oxford.

Cliff, G., and Lorimer, G. W. (1975) *J. Microsc.* **103,** 203–7.

Guidotti, C. V., Cheney, J. T., and Conatore, P. D. (1975) *Am. Mineral.* **60,** 849–53.

Helgeson, H. C., Delaney, J. M., Nesbitt, H. W., and Bird, D. K. (1978) *Am. J. Sci.* **278,** 1–229.

Hobbs, L. W. (1983) *Radiation damage.* In *Quantitative Electron Microscopy.* Proc. 25th Scottish Universities Summer School in Physics, 1983.

Jaeger, J. C. (1957) *Am. J. Sci.* **255,** 306–18.

Kwak, T. A. P. (1968) *Geochim. Cosmochim. Acta.* **32,** 1222–9.

McClachlan, D. (1978) *Can. Mineral.* **16,** 415–25.

McGill, R. J., and Hubbard, F. H. (1981) In *Qualitative microanalysis with high spatial resolution* (G. W. Lorimer, M. H. Jacob, P. Doig, eds.). The Metals Society.

Nakajima, Y., and Ribbe, P. H. (1981) *Am. Mineral.* **66,** 142–7.

Putnis, A., and McConnell, J. D. C. (1980) *Principles of mineral behaviour.* Blackwell Scientific Publications.

Roberts, J. L. (1975) *Geol. Soc. Am. Abst. with Programs,* **6–7,** 844–5.

Robie, R. A., Hemingway, B. S., and Fisher, J. R. (1978) *U.S. Geol. Survey. Bull.* 1452, 452 pp.

Smith, J. V., and Ribbe, P. H. (1966) *J. Geol.* **74,** 197–217.

Veblen, D. R., and Buseck, P. R. (1981) *Am. Mineral.* **66,** 1107–34.

—— and Ferry, J. M. (1984) Ibid. **68,** 1160–8.

Whittaker, E. J. W. (1981) *Crystallography.* Pergamon Press, Oxford.

Wirth, R. (1985) *Neues Jahrb. Mineral. Abh.* **152,** 101–12.

[*Revised manuscript received 5 February 1986*]